Experimental and numerical study of one-sided branch plate-to-circular hollow section connections

M.M. Hassan [*], H. Ramadan [a], M. Abdel-Mooty [b] and S.A. Mourad [c]

Department of Structural Engineering, Cairo University, Gamaa Street, Giza, Egypt

Abstract.   Connections to circular hollow steel sections (CHS) are considered one of the most complex and time consuming connections in steel construction. Such connections are usually composed of gusset plates welded to the outside of the steel tube or penetrating the steel tube. Design guides, accounting for the effect of connection configuration on the strength of the connection, are not present. This study aims to investigate, through experimental testing and a parametric study, the influence of connection configuration on the strength of one sided branch plate-to-CHS members. A notable effect was observed on the behavior of the connections due to its detailing changes with respect to capacity, failure mode, ductility, and stress distribution. A parametric study is performed using the calibrated analytical model to include a wider range of parameters. The study involves 26 numerical analyses of finite element models including parameters of the diameter-to-thickness (D/t) ratio, length of gusset plate, and connection configuration. Accordingly, a modification to the formulas provided by the current design recommendations was suggested to include connection configuration effects for the one sided branch plate-to-CHS members.

Keywords: branch plate; circular hollow section; connection; steel structure; tube

1. Introduction

CHS sections have many aesthetical and economical advantages. However, the complexity of their connections makes their use limited. There are many studies dealing with gusset plate construction details. The possible connection configurations include longitudinal single plate connection, through plate connection, stiffened plate connection, and transverse plate connection (Kurobane *et al*. 2004, Lu *et al*. 1994, Martinez-Saucedo and Packer 2009, Wardenier *et al*. 2008).

The strength of gusset plate connection capacity has been considered for circular hollow steel sections, rectangular hollow steel sections, and elliptical hollow steel sections. The effect of different loading cases, static and dynamic loading, was also addressed by several researchers (Elghazouli and Packer 2014, Martinez-Saucedo *et al*. 2008, Shen *et al*. 2013).

The CIDECT CHS design guidelines (2008) determine the plate connection capacity

---

[*]Corresponding author, Assistant Professor, E-mail: mahamoddather@eng.cu.edu.eg
[a] Assistant Professor
[b] Associate Professor
[c] Professor

considering two possible failure modes: chord plastification and chord punching shear failure. The formulas used for design in case of longitudinal plates are:

$$\text{Chord plastification:} \quad N_1^* = Q_u.Q_f.f_{yo}.t_o^2 / \sin \theta_1 \tag{1}$$

$$\text{Chord punching:} \quad N_1^* = 1.16 h_1.f_{yo}.t_o / \sin^2 \theta_1 \tag{2}$$

$$Q_u = 5(1 + 0.4\eta) \tag{3}$$

$$Q_f = (1 - n)C_1 \tag{4}$$

Where Q_u is a partial design strength function accounting for the effect of geometric properties, Q_f is the chord stress function that accounts for the chord normal stress in the connecting face, f_{yo} is the yield strength of the column, t_o is the thickness of the CHS column, θ_1 is the inclination of the bracing member to the axis of the CHS column, η is the ratio of brace member depth to the chord width, D is the diameter of the CHS column, C_1 is a coefficient in chord stress functions, and h_1 is the depth of the branch plate.

The above formulas are deduced for connections with plates at two sides. CIDECT CHS design guidelines (2008) stated that using these formulas for connections with plate at one side yields conservative results. It is also observed that there are no concise formulas for the resistance of the penetrating through connection. Kurobane *et al*. (2004) recommended using the same formula for the plastification resistance; while doubling the value for the punching resistance. Voth and Packer (2012a, b, c) proposed modifications to the above formulas to account for the effect of skew angle based upon an extensive finite element study. It can be noticed that design formulas accounting for connection configurations are rare.

The main goal of this paper is to present the results obtained from an experimental program carried out to investigate behavior and strength of different configurations of one-sided branch gusset plate to CHS columns connection under the action of compressive loading between zero and a value increasing till the capacity of the connection. The loads are applied parallel and perpendicular to the columns axis creating shear and compression on the gusset plates in a compressive cyclic loading pattern. Details of the experimental work are listed in Hassan *et al*. (2013) and Hassan *et al*. (2014a, b). The data extracted from the tests are used to perform a parametric study to address the effect of various parameters. It is also aimed to study the effect of connection detailing on its behavior, load capacity and failure mode which are considered as key aspects for the development of design provisions for such connections. Accordingly, modifications to the CIDECT CHS design guideline (2008) formulas are proposed based on the numerical study results.

2. Experimental program

2.1 Specimen details

Two test units were designed to investigate the behavior, load capacity, and failure mode of branch plate-to-CHS columns and were tested till failure in the laboratory of the American University in Cairo. The results were also used to verify the constructed numerical models. The

difference between the two specimens was in the direction of load application. All other parameters that may affect the connection behavior such as pipe size, pipe thickness and plate edge distance were fixed. Figs. 1 and 2 show the general layout and the main dimensions of the tested connection. The main dimensions of the tested specimens are summarized and listed in Table 1. The listed data include the pipe diameter, D, shell thickness, t, and the thickness of the connection gusset plate, t_g.

The connection subassembly consisted of a small part of circular pipe fabricated from 114 mm diameter, which represents a part of CHS column, connected to stiffened steel seats by bolting. The length of specimens was fixed to be 680 mm. The distance between the gusset plate edge and all the specimens' ends was 90 mm. This distance was chosen as the least probable distance in order to decrease the moment applied on the steel tube to the least value. Each specimen was fixed to the strong floor using two anchor bolts. Maximum allowable fillet weld sizes were used to join the gusset plate to the steel tube that performed using E70 electrodes. To study the adherence and compatibility of connection design to seismic specifications, the connections were stronger than the CHS column.

2.2 Test configuration

The supporting system is designed to be compatible with the lab facilities available such as strong wall, strong floor, and rigid frame. The hydraulic mechanical actuator with capacity 1400 kN and ± 400 mm stroke was supported by the strong wall from one of its sides. It was attached to the specimen from the other side through a thick plate and two angles connected to the end of the connection gusset plate. The compression load is applied on the specimens in two different directions, parallel and perpendicular compression to the specimen axis (Fig. 2), to simulate the
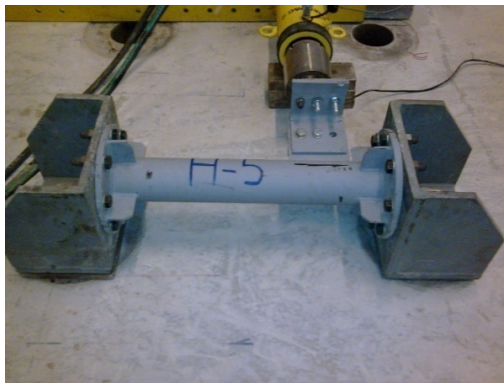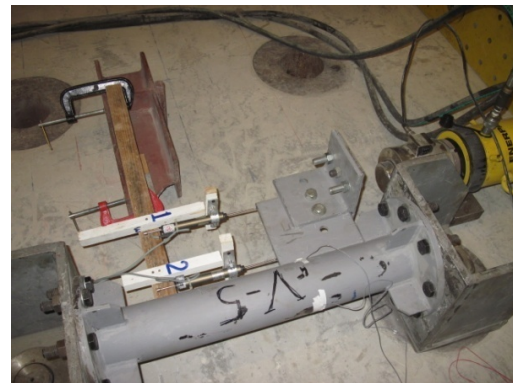
(a) Test Unit H-5   (b) Test Unit V-5

Fig. 1 General view of the test set-up

Table 1 Test unit summary of properties

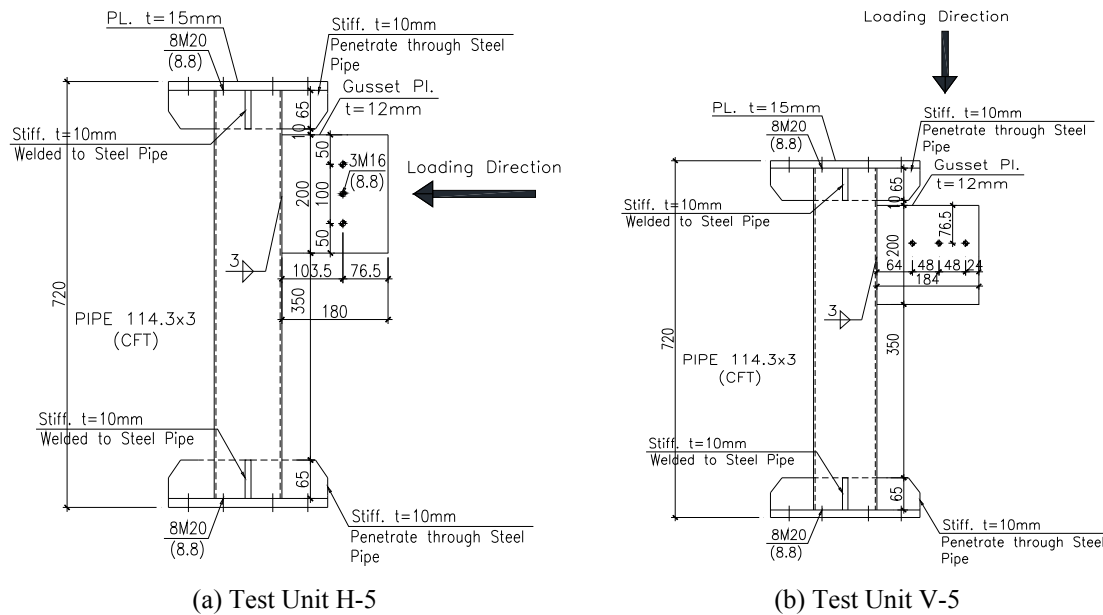| Test unit	D (mm)	t (mm)	t_g (mm)	Loading direction
H-5	114.3	3	12	Perpendicular to specimen axis
V-5	114.3	3	12	Parallel to specimen axis

(a) Test Unit H-5　　　　　　　(b) Test Unit V-5

Fig. 2 Main dimensions of tested specimens

vertical and horizontal components of the forces that can be applied on the connections. It can be seen that specimens were supported at one central point at each end which resulted in rotating of the whole specimen around these points. Therefore, the additional rotation and displacement are subtracted from the results. Such calculations depend upon the edge LVDTs and the measured slip of the anchor bolts. First, the slippage from the anchor bolts was deduced from the LVDTs measurements. Afterwards, the measurements of the edge LVDTs were used to calculate the rotation at ends while considering the center of rotation at the anchor bolt location. Great care was given to leveling of the specimens to ensure that it was correctly aligned during testing.

2.3 Material properties

The tested specimens included steel columns pipes and steel plates. Five test coupons were taken from the pipes and gusset plates to evaluate the mechanical properties through tensile tests. Four of them were cut out from the ends of steel pipes composing the columns after the completion of the experiments and the last was taken from the gusset plates. The principle material properties measured in these tests are reported in Table 2. Connecting angles and gusset plates were made of St 37-2 [A36].

2.4 Instrumentation

The instrumentation of the specimens was designed to determine the applied loads, measure deformations along the specimen, and quantify the internal stresses of the specimens. Electrical strain gages, with 6 mm gauge length, were glued to the steel tube at the midpoint of the gusset plate to measure strains at the connection zone during different stages of loading. Two strain gauges were used for each specimen.

Table 2 Mechanical properties of steel shapes

Specimen No.	Yield stress (MPa)	Ultimate stress (MPa)	Elongation (%)
Specimen-1	278.8	347.4	18.8
Specimen-2	293.8	356.6	30
Specimen-3	267.1	347.4	33.75
Specimen-4	300.6	362.7	25
Specimen-5	337.9	384.7	26.0

Linear variable displacement transducers (LVDTs) were used to measure displacements at different locations of specimens as illustrated in Fig. 3. For the test unit loaded perpendicular to the unit axis, four LVDTs are used: at the two end plates (LVDT-1 and LVDT-4), at the middle of the gusset plate (LVDT-2), and at the edge of the gusset plate (LVDT-3). For the test unit loaded parallel to the unit axis, two LVDTs (LVDT-1 and LVDT-2) are used at the ends of the gusset plate. The value of the applied load was measured directly by the load cell attached to the actuator.

2.5 Loading procedure

At the beginning of the test, a small force was applied and increased gradually, meanwhile, the data acquisition system was observed to ensure that the readings were reasonable. The applied compression load was 0.5 kN/sec, which was chosen as the slowest possible loading rate in order to preclude any impact or dynamic effects and guarantee better observation of the testing procedure while preserving a reasonable testing period. Initially, the forces were increased by 2.5 kN per each successive cycle then drops to zero till reaching 25 kN. Then the load was increased accordingly with 5 kN pro each cycle until the specimens showed large deformations or failure of one of the structural elements. All the CHS columns specimens are subjected to the same loading history which included successive different displacement cycles according to the stepwise loading protocol as shown in Fig. 4.
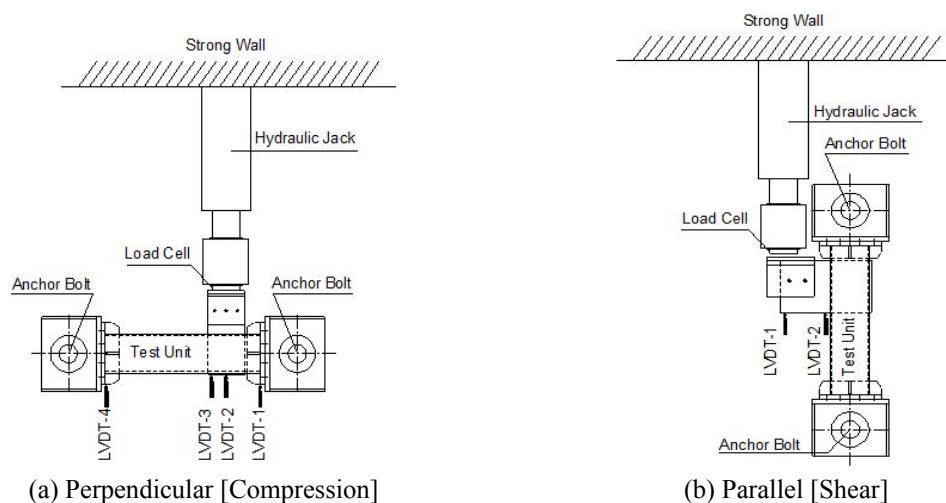

(a) Perpendicular [Compression]   (b) Parallel [Shear]
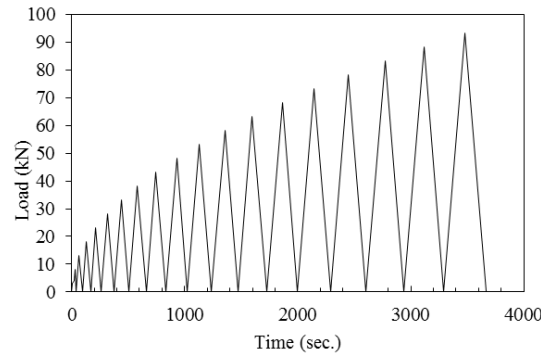
Fig. 3 Plan of Test Set-up for Loaded Specimens

Fig. 4 Test units loading pattern

3. Results

The experimental results showing the specimens' behavior, load-displacement curves, failure patterns and strain measurements of the tested connection subassemblies are outlined and discussed in the following sections.

3.1 Load – Displacement curves

The displacement for the specimens loaded in the perpendicular direction was calculated at the middle of the gusset plate after removing the deformation resulting from the rotation of the test unit ends around the fixation point. On the other hand, the displacement for the specimens loaded in the parallel direction was calculated at the middle of the gusset plate as the average of the readings of LVDT-1 and LVDT-2 shown in Fig. 3(b). Fig. 5 shows the load-displacement curves for the tested subassemblies. It can be observed that the two specimens showed a linear behavior followed by a nonlinear behavior as the loading increased. The nonlinear behavior developed at different loading levels according to the direction of loading and the details of the specimens. For test unit H-5, the nonlinear behavior started at load level around 40 kN. For test unit V-5, the nonlinear behavior of specimens started at loading value equal to 27 kN.
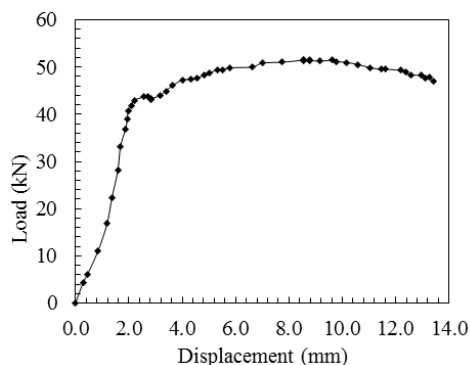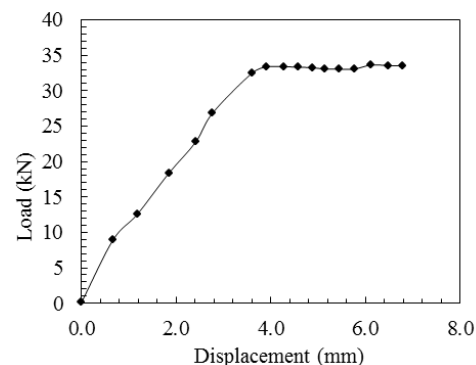
(a) Test Unit H-5   (b) Test Unit V-5
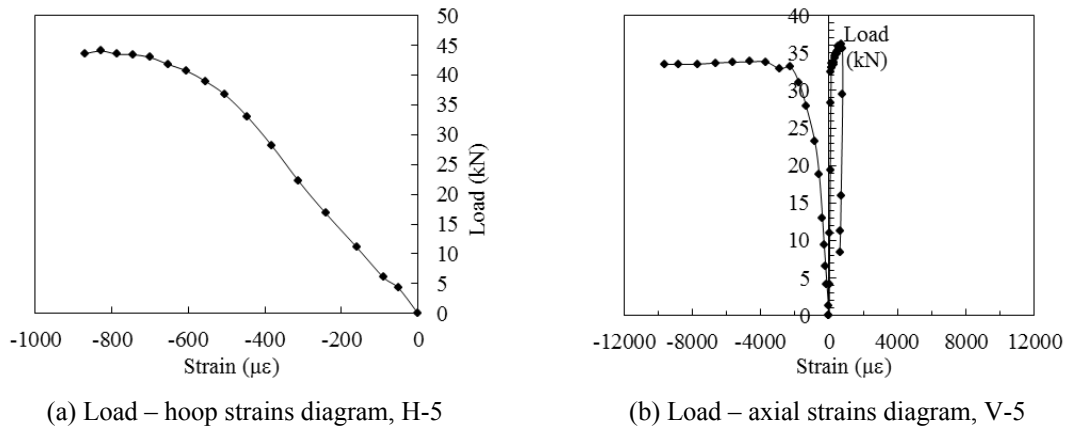
Fig. 5 Load – displacement diagram

(a) Load – hoop strains diagram, H-5   (b) Load – axial strains diagram, V-5

Fig. 6 Load – strain diagram

3.2 Strain measurements

The hoop strain response for test unit H-5 is illustrated in Fig. 6(a). Although tensile hoop strains were expected in CHS sections, tested specimens showed negative values that denote compressive stresses rather than tensile. This can be attributed to the absence of axial load on the CHS column and the direction of loading which imposes compression forces within the zone of connection. Fig. 6(b) shows the axial strains measured at both sides of specimens for test unit V-5. The compressive strains were larger than the corresponding tensile ones due to deformation of the pipe under the gusset plate.

3.3 Failure modes

A significant and sudden loss of resistance was observed for the two test units due to large plastic deformations observed at the gusset plate zone and beneath the applied load as shown in Fig. 7.
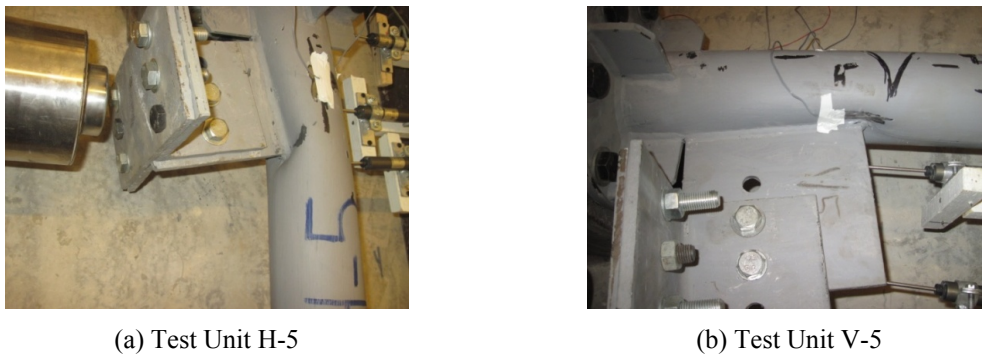

(a) Test Unit H-5   (b) Test Unit V-5

Fig. 7 Failure modes

4. Numerical modeling

ANSYS finite element program (1998), version 11, software package is used to build the 3-D models representing the connections of the hollow steel subassemblies. The main elements which have to be modeled are the steel tube and the concrete and also the end seats. Selection of elements and meshing size is decided after several runs to obtain accurate results with reasonable computing time. The steel seats that were used to support the specimens are modeled using eight-node 3D (SOLID45) elements. The steel tubes were modeled using four-node 3D shell (Shell181) elements. Fig. 8 shows the modeling of the different parts comprising the model for the different connections configuration. Details of the three connection configurations considered in the current study are shown in Fig. 9. Detail 1 includes gusset plate fitting within slots in the steel tube. Meanwhile, Detail 2 refers to connections are similar to detail 1 with an additional gusset plate welded perpendicular to the penetrating gusset plate. Finally, detail 3 refers to connections with gusset plate welded directly to the steel tube. Fig. 10 shows a general view of the finite element model including the mesh structure.
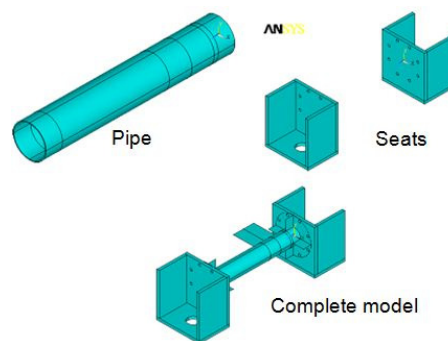
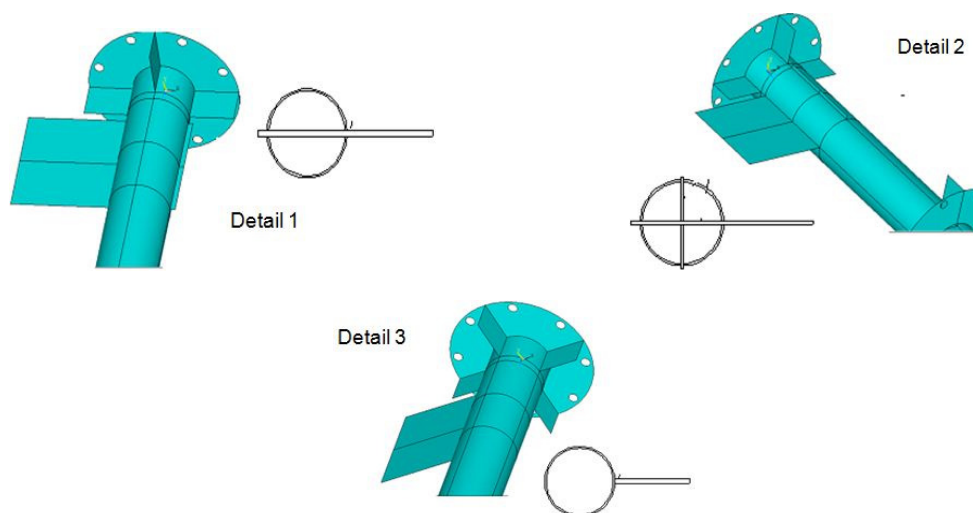

Fig. 8 General layout of the model

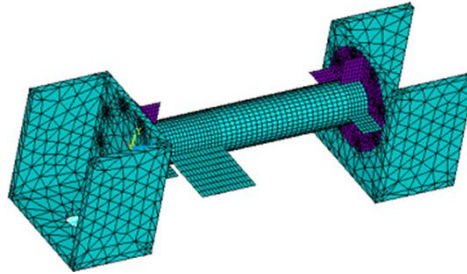Fig. 9 Modeling of the connection configuration

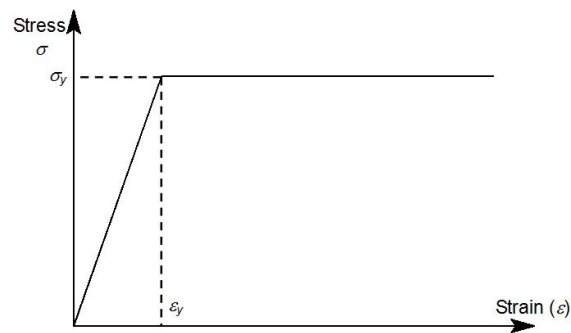Fig. 10 Finite elements modeling of the subassemblies

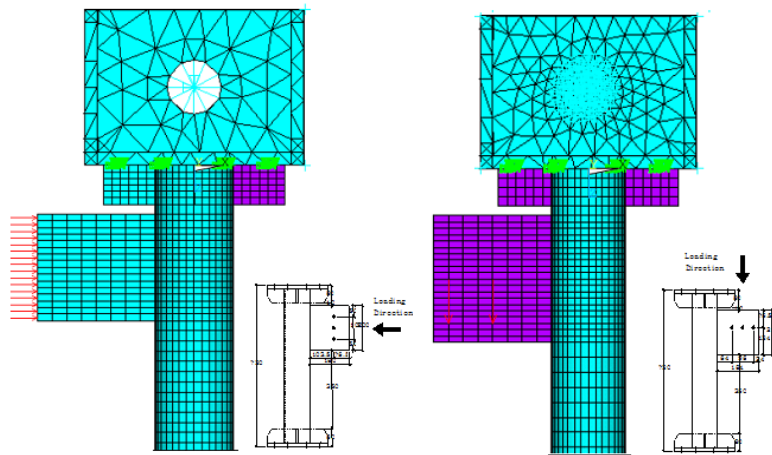Fig. 11 Steel elastic-perfectly plastic stress-strain curve

Fig. 12 Connection loading and boundary conditions

4.1 Material properties

The steel elements were modeled as elastic perfectly plastic materials with yield stress 240 MPa as illustrated in Fig. 11. This value is based on tension tests results carried out by the others (Hassan *et al*. 2013). The modulus of elasticity, E_s, and Poisson's ratio, v_s, were taken 200,000 MPa and 0.3, respectively. Von-Misses yield criteria were used to defined the yield surface and no strain-hardening was assumed.

4.2 Loading and boundary conditions

The CHS assembly is connected to the end steel parts using bolts. Bolts were modeled by coupling nodes located at the interface of the holes at both ends. The two anchor bolts were modeled by constraining the point at the middle of the bolt. The supports were such that the end steel supports can rotate around this point as observed during the experimental part. The forces are applied across the tip of the gusset plate in order to simulate the experimental situation. Fig. 12 shows load application on the gusset plate.

5. Results

5.1 Verification of models

The 3-D models are built to resemble the subassemblies used in the experimental program. Hence, the numerical models are verified using the experimentally-obtained results, and then the models are developed in order to expand the parametric data base. In this section, the numerical and experimental results are compared in order to prove the validity of the models for extended analysis. Fig. 13 shows the experimental and numerical results. It can be noted that there are some differences between the numerical and experimental responses. The relative error for test unit H-5 between the numerical and experimental results is 0.4%, 4.8%, 4.2%, and 3.4% for the yield load, ultimate load, initial stiffness, and post-yield stiffness, respectively. For test unit V-5, the relative error is 4.5%, 2.8%, 3.6%, and 3.2% for the yield load, ultimate load, initial stiffness, and post-yield stiffness, respectively. The differences are mainly attributed to the uncertainty in the material properties and the approximations considered in modeling.

Fig. 14 indicates good correlation between the experimental and numerical results with respect to the stresses patterns and deformed shapes. As can be noted, the Von Misses nodal stresses exhibit high stress values at the location of failure of connection noted in the experimental program.

5.2 Parametric analysis study

The parametric study is performed using the calibrated models to investigate the effect of
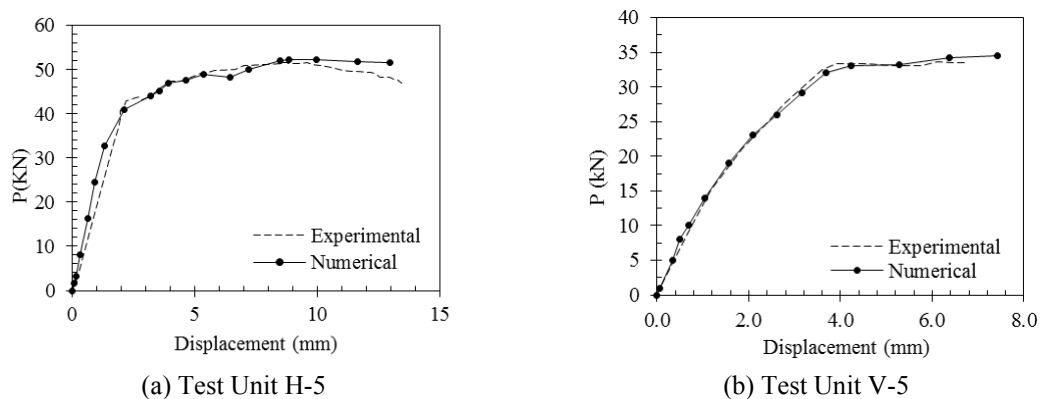

(a) Test Unit H-5   (b) Test Unit V-5

Fig. 13 Experimental and numerical results

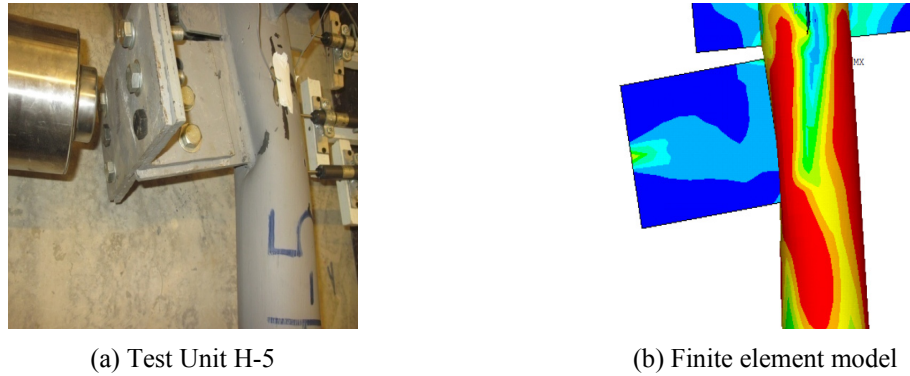(a) Test Unit H-5   (b) Finite element model

Fig. 14 Comparison of deformed shape for specimen vs. actual test unit

different parameters which have been covered by the experimental on the different characteristics of the beam-brace-column connection. The studied independent parameters used in the study can be summarized as follows:

- Steel tube slenderness ratio (D/t).
- Length of gusset plate as per Van der Vegte (2007) and Voth and Packer (2012c).
- Different connection configurations.

The parametric study was established by varying the value of each independent parameter separately whereas all other parameters were kept unchanged. The independent parameters were varied within practical limits and the selected range is listed in Table 3.

5.3 Analysis of results

The analysis of different models is conducted in order to cover the various cases listed in Table 3. The results include the load-deformation curves of the connection and the Von Misses nodal stresses for the steel and concrete elements. The load-deformation curves are used to determine the yield and ultimate capacities of the connection as well as the yield and ultimate deformation. The ultimate capacity (P_u) is defined as proposed by Lu *et al*. (1994) as the load corresponding to a deformation of 3% of the diameter which is acceptable for connections that do not exhibit a peak load. The yield load (P_y) is taken at the location where the tangent stiffness reduces to one third of the initial stiffness as proposed by Kamba and Taclendo (1998).

Figs. 15(a)-(d) exhibit the influence of the gusset plate length on the yield, ultimate strength, initial stiffness, and post-yield stiffness of the connection. For increase of 50% in the gusset plate

Table 3 Range of the studied independent parameters

| Parameter	Studied Range
D/t	20, 30, 40, 50, 60
Diameter (mm)	114.3, 200, 300 and 400 mm
Length of gusset plate	200, 300, and 400mm
Connection Configuration	Detail (1) through Detail (3) [Fig. 9]

length, the ultimate strength of connection increases by 10.9%, 5.8%, and 13.9% for details 1, 2, and 3, respectively. Meanwhile, doubling the gusset plate length resulted in enlarging the ultimate strength by 25.0%, 20.1%, and 30.8% for the same types of connections. It is clear that the effect of increasing the gusset plate length on the ultimate strength is more pronounced in connection detail 3; meanwhile the least effect was exhibited in connection detail 2. This clarifies that in connections having more force application locations at the connection zone, the effect of increasing the gusset plate length is less evident. For increase of 50% in the gusset plate length, the connection yield strength increases by 13.5%, 8.1%, and 8.6% for details 1, 2, and 3, respectively. Meanwhile, doubling the gusset plate length resulted in enlarging the yield strength by 23.1%, 21.6%, and 28.6% for the same types of connections. It is generally observed that the relation of the ultimate and yield strength versus the gusset plate length is linear. For increase of 50% in the gusset plate length, the initial stiffness increased by 7.9%, 16.5%, and 14.2% for details 1, 2, and 3, respectively. Meanwhile, doubling the gusset plate length resulted in enlarging the initial stiffness by 12.1%, 41.5%, and 45.3% for the same types of connections. The post-yield stiffness increased for connection detail 2 by percentages equal to 46.0% and 61.3% for increase in the gusset plate length of 50% and 100%, respectively. For the rest of connection details, the post-yield stiffness did not show a clear relation to the gusset plate length.
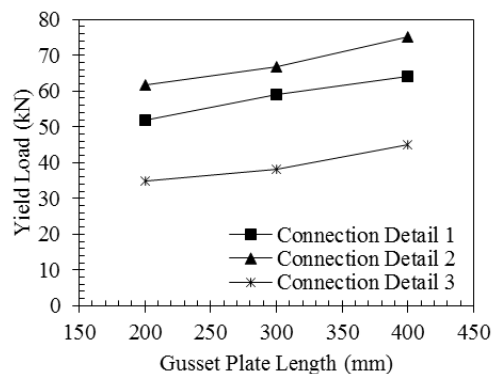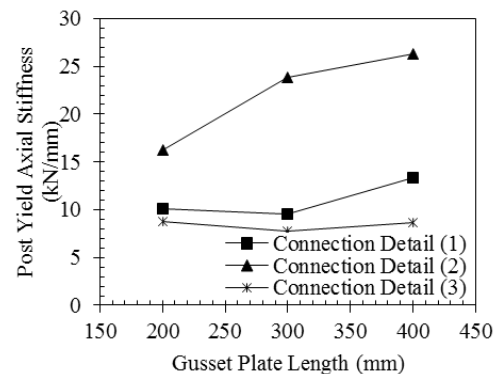

(a) Yield Load - Gusset plate length
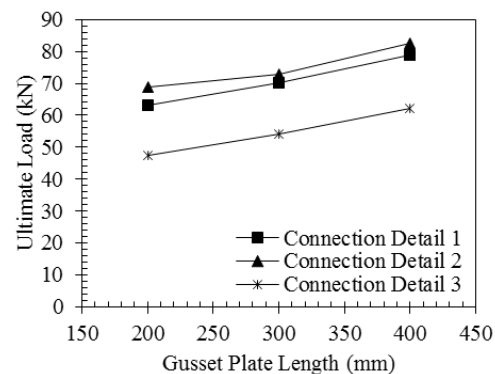
(b) Ultimate Load - Gusset plate length
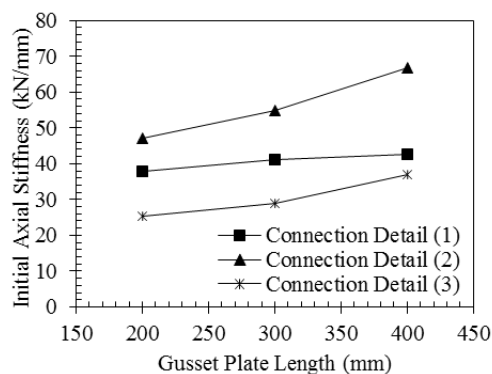
(c) Initial stiffness- Gusset plate length

(d) Post yield stiffness- Gusset plate length

Fig. 15 Influence of gusset plate length

Figs. 16(a)-(d) show the yield and ultimate strength versus the *D*/*t* ratio for the different studied diameters. The influence of varying *D*/*t* ratio on the different characteristics of the connection is generally the same for the studied connection since decreasing the *D*/*t* ratio results in increasing the ultimate strength, yield strength, initial stiffness, and post-yield stiffness. The rate of increase in the ultimate strength is nearly linear and increases as larger diameters are considered. The connection ultimate capacity increases as *D*/*t* ratio decreases. Comparing to the results when using *D*/*t* equals to 60, the percentage of such increase are 41%, 30%, 30% and 38% when the *D*/*t* ratio decreases to 50 for diameters 114.3 mm, 200 mm, 300 mm, and 400 mm, respectively**.** Meanwhile, the percentage ratios of such increase are 80%, 79%, 57%, and 100% for the same diameters when decreasing *D*/*t* ratio decreases to 40. Such increases reach to 2.7, 2.9, 2.8, and 2.8 times for diameters 114.3 mm, 200 mm, 300 mm, and 400 mm, respectively, for *D*/*t* ratio equal to 30 when compared with *D*/*t* value 60 results. For *D*/*t* ratio equal to 20, the increase in ultimate strength reaches 4.3, 4.5, 5.0, and 3.8 times for diameters 114.3 mm, 200 mm, 300 mm, and 400 mm, respectively, when compared with *D*/*t* value 60 results. The connection yield capacity increases as *D*/*t* ratio decreases. Compared to results of connection with *D*/*t* equals to 60, the average rate of increase is 1.5 or 2 times when the *D*/*t* ratio decreases to 50 or 40, respectively. However, the average rate of increase is about 3.4 or 6.7 times when decreasing the *D*/*t* to 30 or 20, respectively. The initial stiffness increased by an average ratio equal to 1.2, 1.6, 2, and 2.8 when decreasing the
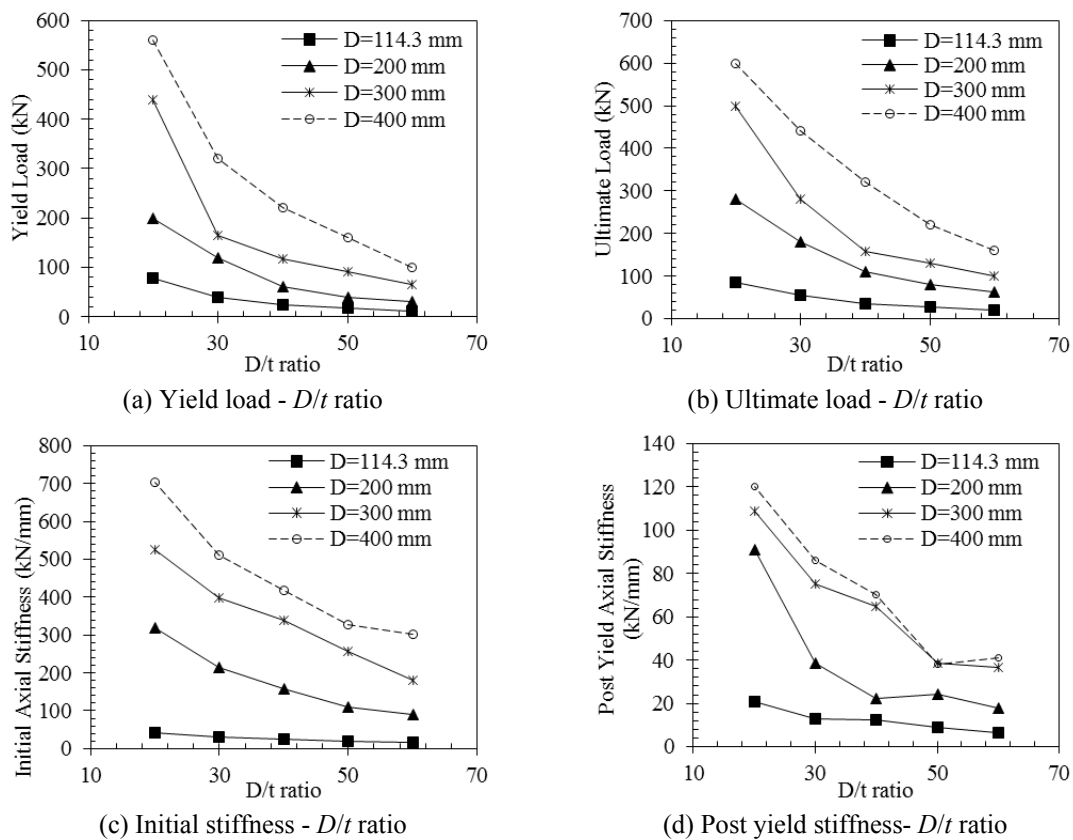

(a) Yield load - *D*/*t* ratio

(b) Ultimate load - *D*/*t* ratio

(c) Initial stiffness - *D*/*t* ratio

(d) Post yield stiffness- *D*/*t* ratio

Fig. 16 Influence of *D*/*t* ratio

(a) Yield load - Connection detail

(b) Ultimate load - Connection detail

(c) Initial stiffness - Connection detail
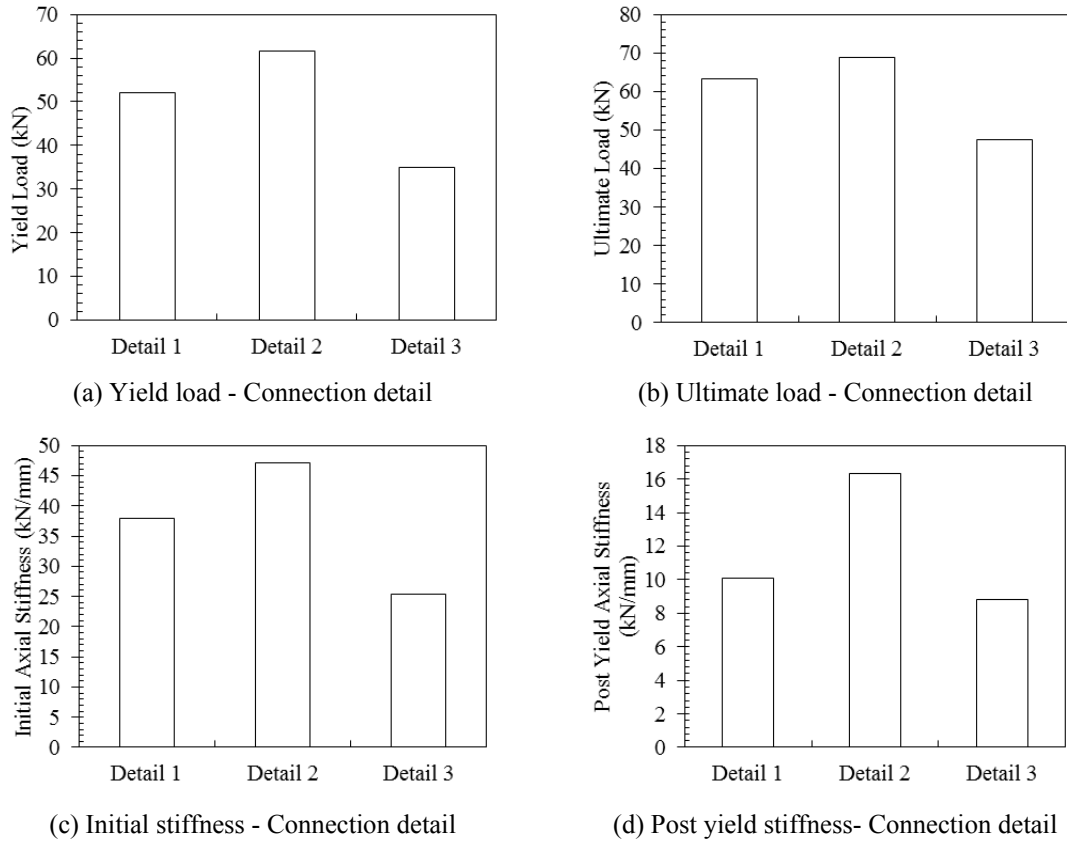
(d) Post yield stiffness- Connection detail

Fig. 17 Influence of connection detail

D/t ratio from 60 to 50, 40, 30, and 20, respectively. The rate of increase in the initial stiffness of the connection is almost linear for the four studied diameters. The post-yield stiffness also increases as the *D/t* ratios decreases. For diameter equal to 114.3 mm, the rate of increase was insignificant. For 200 mm diameter hollow steel tube and compared to pipe with *D/t* equals to 60, the average ratios of the post-yield stiffness are 1.2, 1.7, 2.1, and 3.6 times at *D/t* ratios equal to 50, 40, 30, and 20, respectively.

The effect of the studied connection detail on the yield and ultimate strength is illustrated in Figs. 17(a)-(d). Connection detail 2 exhibits the highest values for the different studied quantities. This shows that adding additional plate in hollow steel sections would generally increase the strength and stiffness of the connection. Using one gusset plate penetrating through the column (detail 1) increases the ultimate strength, yield strength, initial stiffness, and post-yield stiffness by 33%, 48%, 50%, and 15% comparing to connections with gusset plate welded to the outside steel tube shell (detail 3). Using two gusset plates intersecting at the connection zone (detail 2) increases the ultimate strength, yield strength, initial stiffness, and post-yield stiffness by 45%, 76%, 85%, and 85% comparing to connections with gusset plate welded to the outside steel tube shell (detail 3).

5. Proposed formulas

The experimental and the numerical results are used to develop a mechanical model that can capture the behavior of gusset plate connections to hollow steel members. The results are used to assess the behavior of gusset plate connections to hollow steel sections from one side while accounting for the different configurations of the connection. This is done based upon the trilinear model proposed by Kamba and Taclendo (1998). Fig. 18 shows a schematic view of the model. The model of the load-deformation curve of the connection is a trilinear model connecting the origin, point A, B and point C. The coordinates of the main points is summarized in Table 4. P_{max} and P_y refer to the maximum and yield loads. Δ_{max} and Δ_y are the maximum and yield local deformations. (Kamba and Taclendo 1998).

The yield strength, ultimate strength, initial stiffness, and post-yield stiffness were determined from the numerical simulations and considering the different parameters. The yield load values for hollow steel sections are compared to the values computed according to Eq. (5) as per the CIDECT CHS design guidelines (2008). In our case, Q_f and $\sin\theta_1$ are equal to unity. Hence, the formula is reduced to

$$P_y = Q_u \cdot f_y \cdot t^2 \tag{5}$$

The quantity (Q_u) is calculated according to Eq. (3) as per the CIDECT CHS design guidelines (2008). Meanwhile, the results from the numerical analyses are used to calculate $Q_{u(num)}$ according to Eq. (5).

Table 5 lists the results for connection detail 3 only. It can be seen that the value of Q_u given by the CIDECT design guide (2008) is generally conservative. Accordingly, it is proposed to modify

Fig. 18 Model of load-displacement curve
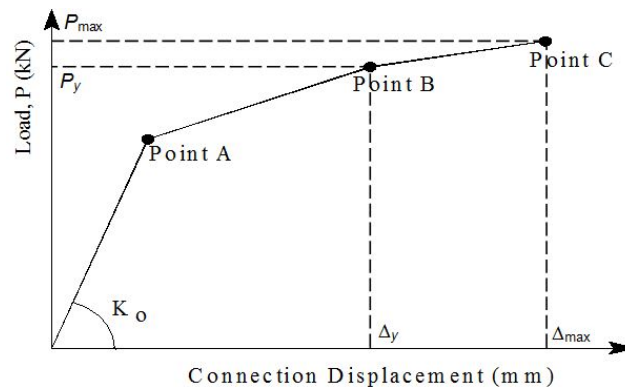
Table 4 Main coordinates of the proposed model

Point	Load (P)	Displacement (Δ)
A	$2/3P_y$	$2/3P_y/K_o$
B	P_y	Δ_y
C	P_{max}	Δ_{max}

M.M. Hassan, H. Ramadan, M. Abdel-Mooty and S.A. Mourad

Table 5 FEM results for hollow steel sections

Gusset pl. length (mm)	D (mm)	t (mm)	$Q_{u(Design)}$	$Q_{u(num)}$	$Q_{u(num)}/ Q_{u(Design)}$	P_{max}/P_y
200	114.3	3.00	8.50	13.64	1.60	1.35
300	114.3	3.00	10.25	14.81	1.44	1.24
400	114.3	3.00	12.00	17.54	1.46	1.55
200	114.3	1.91	8.50	12.06	1.42	1.90
200	114.3	2.86	8.50	12.76	1.50	1.31
200	114.3	5.72	8.50	10.08	1.19	1.23
200	200.0	3.33	7.00	11.25	1.61	2.05
200	200.0	5.00	7.00	10.00	1.43	1.83
200	200.0	10.00	7.00	8.33	1.19	1.59
200	300.0	5.00	6.33	10.67	1.68	1.33
200	300.0	7.50	6.33	8.67	1.37	1.34
200	300.0	15.00	6.33	8.15	1.29	1.14
300	200	5	8.00	12.00	1.50	1.94
450	200	3.33	9.50	15.03	1.58	1.69
500	200	3.33	10.00	13.53	1.35	1.67
200	114.3	2.286	8.50	14.03	1.65	1.60
200	114.3	3.81	8.50	11.19	1.32	1.41
200	200	4	7.00	10.42	1.49	2.00
200	200	6.667	7.00	11.25	1.61	1.50
200	300	6	6.33	10.42	1.64	1.44
200	300	10	6.33	6.88	1.09	1.70
200	400	6.67	6.00	9.37	1.56	1.60
200	400	8	6.00	10.42	1.74	1.38
200	400	10	6.00	9.17	1.53	1.45
200	400	13.33	6.00	7.50	1.25	1.38
200	400	20	6.00	5.83	0.97	1.07
			Average		1.44	1.53
			St. Dev.		0.19	0.27
			COV		0.13	0.17

modify the formula as follows

$$Q_u = 7.2 * \gamma * (1 + 0.4\eta) \tag{6}$$

$$\eta = h_1 / D \tag{7}$$

Where η is the ratio of brace member depth to the chord width and γ is a proposed factor that accounts for the connection configuration.

Table 6 shows the proposed values for factor (γ) and the ratio between the maximum loading that the connection can sustain and the load at yield. Fig. 19 shows the proposed model with respect to the finite element results.
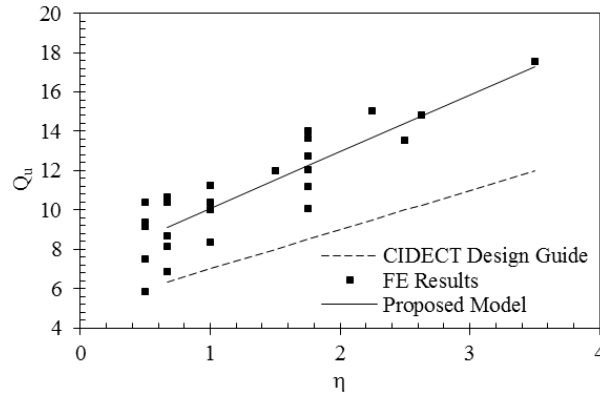
Fig. 19 Correlation of the proposed equation

Table 6 Factor accounting for the connection configuration

Detail type	Factor (γ)	P_{max}/P_y
Detail 1	1.6	1.21
Detail 2	1.4	1.38
Detail 3	1.0	1.54

Table 7 Estimated formulas for the initial and post-yield stiffness

Detail type	K_o/E	K_f/E
Detail 1	$120*(D/t)^{-2}*(h_1/D)$	$25*(D/t)^{-1.8}*(h_1/D)^{0.6}$
Detail 2	$180*(D/t)^{-2}*(h_1/D)$	$50*(D/t)^{-1.8}*(h_1/D)^{0.6}$
Detail 3	$48*(D/t)^{-2}*(h_1/D)$	$8*(D/t)^{-1.8}*(h_1/D)^{0.6}$

The initial and post-yield stiffness formulas are estimated using the least squares method and following the mathematical model proposed by Kamba and Taclendo (1998)

$$K / E = X_1.(D/t)^{X2}.(h_1/D)^{X3}.\varepsilon \tag{8}$$

Where K/E is the ratio between the initial or post-yield stiffness and the elastic modulus of the material; while, ε is the error. The numerical variables X_1, X_2, X_3 are determined by the method of least squares using the finite element results.

After conducting the statistical analysis on the available results, the formulas of the initial and post-yield stiffness are listed in Table 7 considering the different studied detail types.

Fig. 20 shows a comparison of the finite element response versus the estimation provided by the proposed model for a sample of the FEM results. The estimated trilinear response shows good agreement with finite element results.
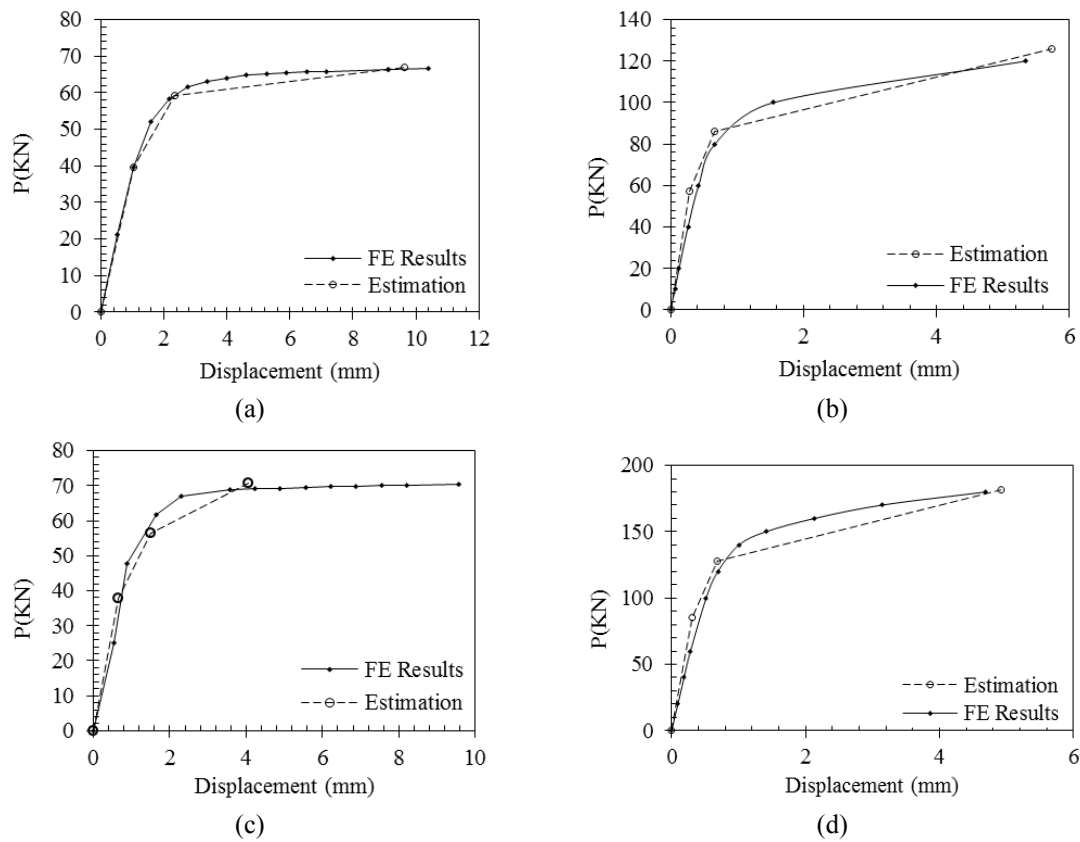
Fig. 20 Comparison between the FE results and the proposed model

6. Conclusions

An experimental investigation was carried out in order to study the behavior of the gusset plate connections. Accordingly, a numerical finite element parametric study simulating different connection configurations was conducted. The behavior of CHS connections was found to be dependent upon the gusset plate length, D/t ratios, and the connection configuration. Formulas given in the CIDECT CHS design guide (2008) are developed based upon the results. The estimated trilinear load-displacement curves provided by the proposed mechanical models showed good agreement with the FE results.

Acknowledgments

References

Elghazouli, A.Y. and Packer, J.A, (2014), "Seismic design solutions for connections to tubular members", *J. Steel Constr*.**, 7**(2), 73-83.

Hassan, M.M., Ramadan, H.M., Abdel-Mooty, M. and Mourad, S.A. (2013), "Experimental study of CFT bracing connections behavior under half-cyclic loading", *Proceedings of the 11th International Conference on Steel*, *Space and Composite Structures*, Qingdao, China, December.

Hassan, M.M., Ramadan, H.M., Abdel-Mooty, M., and Mourad, S.A. (2014a), "Behavior of concenrtrically loaded CFT braces connections", *J. Adv. Res.*, **5**(1), 243-252.

Hassan, M.M., Ramadan, H.M., Naeem, M. and Mourad, S.A. (2014b), "Behavior of gusset plate-T0-CCFT connections with different configurations", *Steel Compos. Struct.*, *Int. J.*, **17**(5), 735-751.

Kamba, T. and Taclendo, C. (1998), "CHS column connections without stiffeners", *Proceedings of the 8th International Symposium on Tubular Structures*, Singapore, August.

Kurobane, Y., Packer, J.A., Wardenier, J. and Yeomans, N. (2004), *Design Guide for Structural Hollow Section Column Connections*, CIDECT, TÜV-Verlag GmbH, Koln, Germany.

Lu, L.H., de Winkel, G.D., Yu, Y. and Wardenier, J. (1994), "Deformation limit for the ultimate strength of hollow sections", *Proceedings of the 6th International Symposium on Tubular Structures*, Melbourne, VA, Australia, December.

Martinez-Saucedo, G. and Packer, J.A. (2009), "Static design recommendations for slotted end HSS connections in tension", *J. Struct. Eng.*, **135**(7), 797-805.

Martinez-Saucedo, G., Packer, J.A. and Christopoulos, C. (2008), "Gusset plate connections to circular hollow section braces under inelastic cyclic loading", *J. Struct. Eng.*, **134**(7), 1252-1258.

Shen, W., Choo, Y.S., Wardenier, J., Packer, J.A. and van der Vegte, G.J. (2013), "Static srength of axially loaded EHS X-Joints with braces welded to the narrow sides of the chord", *J. Constr. Steel Res.*,**88**(1), 181-190.

Swanson Analysis Systems (1998), ANSYS Release 11.0, Houston, USA.

Van der Vegte, G.J., Wardenier, J. and Makino, Y. (2007), "Effect of chord load on ultimate strength of CHS X-joints", *Int. J. Offshore Polar Eng.*, **17**(4), 301-308.

Voth, A.P. and Packer, J.A. (2012a), "Numerical study and design of skewed X-type branch plate-to-circular hollow section connections", *J. Construct. Steel Research*, **68**(1), 1-10.

Voth, A.P. and Packer, J.A. (2012b), "Branch plate-to-circular hollow structural section connections: experimental investigation and finite-element modeling", *J. Struct. Eng.*, **138**(8), 995-1006.

Voth, A.P. and Packer, J.A. (2012c), "Branch plate-to-circular hollow structural section connections. II: X-type parametric numerical study and design", *J. Struct. Eng.*, **138**(8), 1007-1018.

Wardenier, J., Kurobane, Y., Packer, J.A., van der Vegte, G.J. and Zhao, X.L. (2008), *Design Guide for Circular Hollow Section* (*CHS*) *Joints under Predominantly Static Loading*, (2nd Edition), CIDECT, Geneva, Switzerland.

DL